

# Learned Free-Energy Functionals from Pair-Correlation Matching for Dynamical Density Functional Theory

Karnik Ram,<sup>1, e</sup> Jacobus Dijkman,<sup>2, 3</sup> René van Roij,<sup>4</sup> Jan-Willem van de Meent,<sup>3</sup> Bernd Ensing,<sup>2</sup> Max Welling,<sup>3</sup> and Daniel Cremers<sup>1</sup>

<sup>1</sup>*School of Computation, Information and Technology, TU Munich*

<sup>2</sup>*Van't Hoff Institute for Molecular Sciences, University of Amsterdam*

<sup>3</sup>*Informatics Institute, University of Amsterdam, The Netherlands*

<sup>4</sup>*Institute for Theoretical Physics, Utrecht University, The Netherlands*

(Dated: May 30, 2025)

Classical density functional theory (cDFT) and dynamical density functional theory (DDFT) are modern statistical mechanical theories for modeling many-body colloidal systems at the one-body density level. The theories hinge on knowing the excess free-energy accurately, which is however not feasible for most practical applications. Dijkman *et al.* [Phys. Rev. Lett. 134, 056103 (2025)] recently showed how a neural excess free-energy functional for cDFT can be learned from bulk simulations via pair-correlation matching. In this article, we demonstrate how this same functional can be applied to DDFT, without any retraining, to simulate non-equilibrium overdamped dynamics of inhomogeneous densities. We evaluate this on a 3D Lennard-Jones system with planar geometry under various complex external potentials and observe good agreement of the dynamical densities with those from expensive Brownian dynamic simulations, up to the limit of the adiabatic approximation. We further develop and apply an extension of DDFT based on gradient flows, to a grand-canonical system modeled after breakthrough gas adsorption studies, finding similarly good agreement. Our results demonstrate a practical route for leveraging learned free-energy functionals in DDFT, paving the way for accurate and efficient modeling of many-body non-equilibrium systems.

## I. INTRODUCTION

Studying the collective behavior of many-body systems emerging from inter-particle interactions is fundamental in many diverse fields of science, ranging from gas adsorption studies in porous media [1] to semiconductors and protein adsorption [2]. Classical density functional theory (cDFT) [3] is a promising theory for accurately and efficiently modelling such many-body systems at the level of the one-body density profile  $\rho(\mathbf{r})$  in thermodynamic equilibrium. cDFT relies on the existence of an excess free-energy functional  $\mathcal{F}_{\text{exc}}[\rho(\mathbf{r})]$  which describes the inter-particle interactions, accounting for the non-ideal contribution to the total Helmholtz intrinsic free-energy functional  $\mathcal{F}[\rho(\mathbf{r})]$ . This functional is generally unknown and various approximations have been constructed ranging from the mean-field approximation [4] for soft interactions to fundamental measure theory [5] for hard-sphere interactions. More recently, neural functionals learned from Monte Carlo simulations have been proposed [6–10] and exhibit remarkable accuracy.

Dynamical density functional theory (DDFT) [3, 11–13] is an extension of cDFT to describe non-equilibrium systems as a Fokker-Planck equation on the one-body density profile. DDFT has been applied in diverse systems ranging from simple colloidal fluids [11] to plasmas [14] and microswimmers [15]. A recent review of DDFT applications can be found in [16]. Like cDFT, DDFT also relies on the excess free-energy functional and

typically the same equilibrium functional from cDFT is adopted for DDFT under the adiabatic approximation.

In this article, we adopt the neural functional proposed by Dijkman *et al.* [10], that was trained by matching the pair-correlation function from bulk simulations, and evaluate it for DDFT. Despite only having seen bulk densities during training, we show that this functional produces accurate time evolution of 1D inhomogeneous densities on a 3D Lennard-Jones system with planar geometry. We further extend DDFT with a particle source term, based on gradient flows [17, 18], to model grand-canonical systems with non-conserved dynamics. We evaluate this extension on a system inspired by gas adsorption simulations, and observe good agreement with a hybrid Monte Carlo Brownian dynamic simulation.

## II. PAIR-CORRELATION MATCHING

Pair-correlation matching [10] is a method for learning an accurate neural excess free-energy functional  $\mathcal{F}_{\theta, \text{exc}}$  (where  $\theta$  represents neural network parameters) by training exclusively on a dataset of bulk radial distribution functions, rather than from heterogeneous density profiles. The method uses the relationship between the second functional derivative of the excess free-energy functional ( $\delta^2 \mathcal{F}_{\text{exc}} / \delta \rho(z_i) \delta \rho(z_j)$ ) and the direct correlation function  $c^{(2)}(\mathbf{r})$ , which is related to the radial distribution function  $g(r)$  via the Ornstein-Zernike equation ([4], Ch.3), for training. Specifically, a neural network  $\mathcal{F}_{\theta, \text{exc}}$  is trained by optimizing a physics-based regularizer [19], that matches its Hessian ( $\partial^2 \mathcal{F}_{\text{exc}} / \partial \rho_i \partial \rho_j$ ) with the direct correlation function obtained from Monte Carlo simula-

<sup>e</sup> karnik.ram@tum.de

Neural dynamical density functional theory

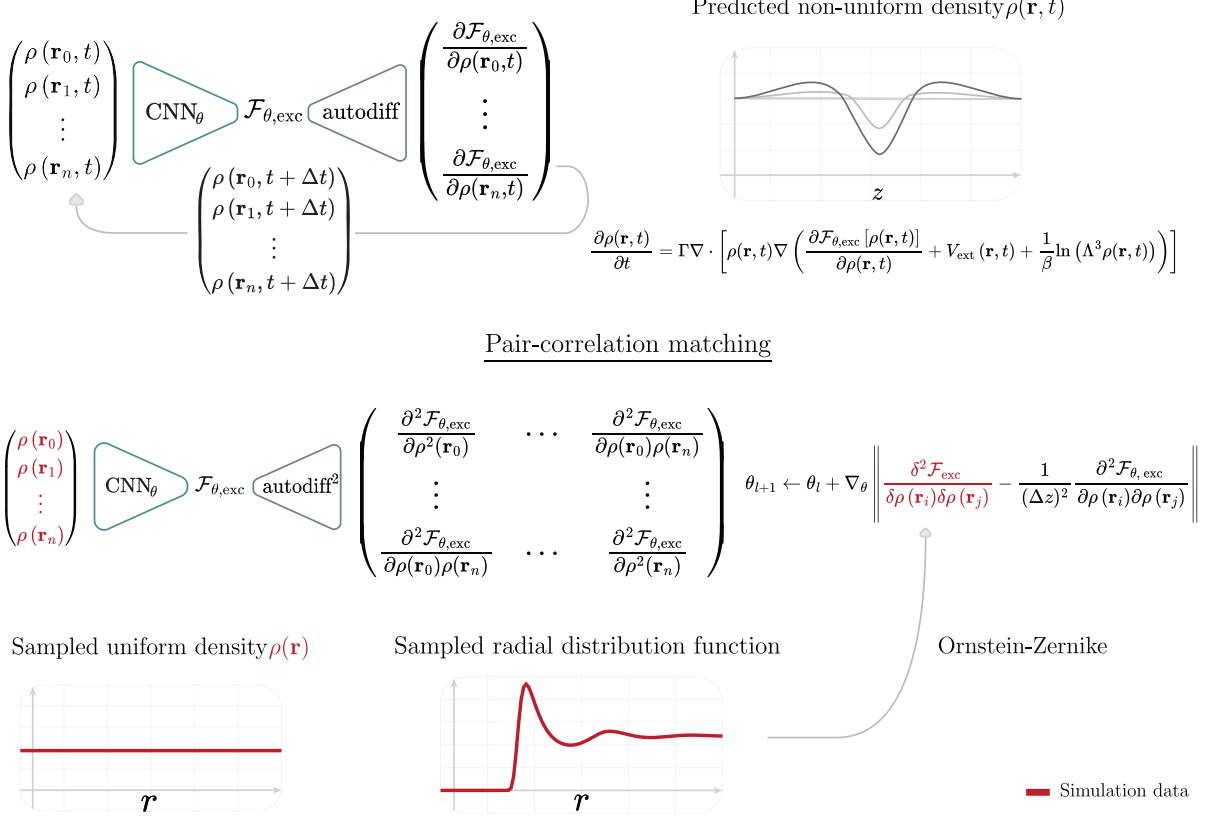


FIG. 1: An overview of the proposed neural DDFT framework, and the pair-correlation matching [10] approach. (Bottom) A neural free-energy functional is trained via pair-correlation matching where its second functional derivative is optimized against the direct pair correlation function computed from simulated uniform bulk densities. (Top) The neural excess free-energy functional  $\mathcal{F}_{\theta, \text{exc}}$  is used for DDFT to time evolve the inhomogeneous particle density  $\rho(\mathbf{r})$  of a 3D Lennard-Jones system with planar geometry via automatic differentiation and numerical integration, towards equilibrium.

tions of homogeneous bulk systems (Fig. 1). This functional is then used in the cDFT scheme to obtain accurate estimates for inhomogeneous equilibrium density profiles under various external fields without having used any inhomogeneous densities during training.

### III. CLASSICAL DYNAMICAL DENSITY FUNCTIONAL THEORY

DDFT was first introduced phenomenologically by Evans [3], and later microscopically derived from the Langevin equations by Marconi and Tarazona [11], and from Smoluchowski equations by Archer and Evans [12]. An extensive review of DDFT fundamentals can be found in [13]. DDFT has the form of a continuity equation where  $\partial_t \rho(\mathbf{r}, t)$  is proportional to the divergence of a vector field as follows,

$$\frac{\partial \rho(\mathbf{r}, t)}{\partial t} = \Gamma \nabla \cdot \left[ \rho(\mathbf{r}, t) \nabla \left( \frac{\delta \mathcal{F}[\rho]}{\delta \rho(\mathbf{r}, t)} \right) \right], \quad (1)$$

where  $\Gamma$  is the mobility coefficient and  $\mathcal{F}[\rho]$  is the intrinsic Helmholtz free-energy functional. This functional consists of three parts,

$$\begin{aligned} \mathcal{F}[\rho] = & \frac{1}{\beta} \int d^3 \mathbf{r} \rho(\mathbf{r}) (\ln(\Lambda^3 \rho(\mathbf{r})) - 1) \\ & + \int d^3 \mathbf{r} \rho(\mathbf{r}) V_{\text{ext}}(\mathbf{r}) + \mathcal{F}_{\text{exc}}([\rho]), \end{aligned} \quad (2)$$

where  $\mathcal{F}_{\text{exc}}([\rho])$  is the excess free-energy functional,  $V_{\text{ext}}$  is the external potential,  $\beta = (1/k_B T)$ , and  $\Lambda$  is the thermal wavelength. Expanding Eq. (1) further we get,

$$\begin{aligned} \frac{\partial \rho(\mathbf{r}, t)}{\partial t} = & \Gamma \nabla \cdot \left[ \rho(\mathbf{r}, t) \nabla \left( \frac{\delta \mathcal{F}_{\text{exc}}[\rho]}{\delta \rho(\mathbf{r}, t)} + V_{\text{ext}}(\mathbf{r}, t) \right. \right. \\ & \left. \left. + \frac{1}{\beta} \ln(\Lambda^3 \rho(\mathbf{r}, t)) \right) \right]. \end{aligned} \quad (3)$$

In the ideal gas limit, where there are no inter-particle interactions i.e.  $\mathcal{F}_{\text{exc}}[\rho] = 0$ , this equation reduces to a drift-diffusion equation where particles only diffuse and

respond to an external potential. The DDFT equation in this standard form, with no velocity or inertial terms, describes purely overdamped dynamics where frictional forces dominate. It also relies on the adiabatic approximation which assumes that the non-equilibrium pair correlation function is equivalent to its equilibrium counterpart at the same one-body density. However, for systems where superadiabatic forces such as memory effects are significant, more advanced frameworks such as power functional theory [20, 21] and superadiabatic DDFT [22] are required. It is also worth noting that since standard DDFT has the form of a continuity equation and conserves the particle number (neglecting the boundaries), it is only a canonical theory in this regard. In practice however it is common to still adopt the same grand-canonical free energy functional from cDFT under the adiabatic approximation. We follow this practice and adopt the equilibrium neural excess-free energy functional from Djokman et al. [10].

#### IV. EXTENSION TO OPEN SYSTEMS

Many practical systems are open to particle exchange with a reservoir—for instance, gas adsorption in porous materials is often modeled using hybrid grand-canonical molecular dynamics simulations [23, 24]. We develop a novel extension of DDFT for such hybrid setups, allowing for particle insertion and removal through a reservoir coupling. This setting was studied before by Thiele *et al.* [25], where a source term was added to model the evaporation of a colloidal suspension into a vapor reservoir. We develop a similar extension, but from a principled Wasserstein-Fisher-Rao gradient flow perspective.

The 2-Wasserstein distance between two densities  $\rho_0, \rho_1$ , defined as

$$W_2^2(\rho_0, \rho_1) = \inf_{\rho \in \Gamma(\rho_0, \rho_1)} \int \rho(\mathbf{r}_1, \mathbf{r}_2) \|\mathbf{r}_1 - \mathbf{r}_2\|_2^2 d\mathbf{r}_1 d\mathbf{r}_2, \quad (4)$$

where  $\Gamma(\rho_0, \rho_1)$  is the space of all joint distributions with marginals  $\rho_0$  and  $\rho_1$ , can also be expressed in dynamical form

$$W_2^2(\rho_0, \rho_1) = \inf_{v_t \in V(\rho_0, \rho_1), \rho_t} \int_0^1 \mathbb{E}_{\rho_t(\mathbf{r})} [\|v_t(\mathbf{r})\|_2^2] dt, \quad (5)$$

where  $V(\rho_0, \rho_1)$  is the set of velocity fields  $v_t$  such that  $(\partial\rho_t/\partial t) = -\nabla_{\mathbf{r}} \cdot (\rho_t(\mathbf{r})v_t(\mathbf{r}))$  with  $\rho_{t=0} = \rho_0$  and  $\rho_{t=1} = \rho_1$ . From this dynamical formulation, which was first proposed by Benamou & Brenier [26], it can be shown that the flow defined by DDFT (Eq. (1)) is in fact the steepest descent on the free-energy functional  $\mathcal{F}[\rho]$  in the space of densities under the 2-Wasserstein distance metric [27].

The space of densities can be endowed with different metrics [17] which correspond to different optimization

dynamics. In particular, the Wasserstein Fisher-Rao distance [18, 28] can be defined by extending Eq. (5) with a growth term,

$$\text{WFR}^2(\rho_0, \rho_1) = \inf_{v_t, \rho_t, g_t} \int_0^1 \mathbb{E}_{\rho_t(\mathbf{r})} [\|v_t(\mathbf{r})\|_2^2 + \lambda g_t(\mathbf{r})^2] dt, \quad (6)$$

and the corresponding continuity equation is updated as  $(\partial\rho_t/\partial t) = -\nabla_{\mathbf{r}} \cdot (\rho_t(\mathbf{r})v_t(\mathbf{r})) + g_t(\mathbf{r})\rho_t(\mathbf{r})$ . It can be shown that the flow that minimizes the free-energy functional  $\mathcal{F}[\rho]$  under this Wasserstein Fisher-Rao metric is given by the following PDE (proof in [18]):

$$\begin{aligned} \frac{\partial\rho_t(\mathbf{r})}{\partial t} = & -\nabla_{\mathbf{r}} \cdot \left( \rho_t(\mathbf{r}) \left( -\nabla_{\mathbf{r}} \frac{\delta\mathcal{F}[\rho_t]}{\delta\rho_t}(\mathbf{r}) \right) \right) \\ & - \frac{1}{\lambda} \left( \frac{\delta\mathcal{F}[\rho_t]}{\delta\rho_t}(\mathbf{r}) - \mathbb{E}_{\rho_t(y)} \left[ \frac{\delta\mathcal{F}[\rho_t]}{\delta\rho_t}(y) \right] \right) \rho_t(\mathbf{r}). \end{aligned} \quad (7)$$

While standard DDFT (Eq. (1)) defines the change of density along a vector field  $v_t(\mathbf{r}) = \nabla_{\mathbf{r}} (\delta\mathcal{F}[\rho]/\delta\rho_t)$ , this PDE also defines the addition and removal of density with a growth term that is proportional to the difference between the local chemical potential  $(\delta\mathcal{F}[\rho_t]/\delta\rho_t(\mathbf{r}))$  and the average chemical potential of the whole system. We replace this average potential with a target chemical potential  $\mu$  to model a grand canonical reservoir and get the following form,

$$\begin{aligned} \frac{\partial\rho(\mathbf{r}, t)}{\partial t} = & \underbrace{\Gamma \nabla \cdot \left[ \rho(\mathbf{r}, t) \nabla \left( \frac{\delta\mathcal{F}[\rho]}{\delta\rho(\mathbf{r}, t)} \right) \right]}_{\text{continuity equation}} \\ & + \underbrace{(1 - \lambda(\mathbf{r})) \Gamma' \left( \mu - \frac{\delta\mathcal{F}[\rho]}{\delta\rho(\mathbf{r}, t)} \right)}_{\text{growth term}} \rho(\mathbf{r}, t), \end{aligned} \quad (8)$$

where  $\lambda(\mathbf{r})$  is a masking function such that  $\lambda(\mathbf{r}) = 0$  for  $\mathbf{r} = \mathbf{r}_i$ , the locations where a particle bath is to be connected, and is equal to 1 elsewhere.  $\Gamma'$  is the corresponding mobility coefficient that controls the rate of the non-conserved dynamics.

We know from cDFT that, at equilibrium,  $\mu$  is given as,

$$\mu = V_{\text{ext}} + \frac{1}{\beta} \ln(\Lambda^3 \rho_{\text{eq}}(\mathbf{r})) + \left. \frac{\delta\mathcal{F}_{\text{exc}}[\rho(\mathbf{r})]}{\delta\rho(\mathbf{r})} \right|_{\rho=\rho_{\text{eq}}}. \quad (9)$$

This relation suggests that the contribution from the external potential  $V_{\text{ext}}$ , ideal gas  $\ln \rho_{\text{eq}}(\Lambda^3 \mathbf{r})$ , and the functional derivative of the excess free energy add up at each position to  $\mu$  at equilibrium. Using this conservation relation we can write the growth-term PDE as,

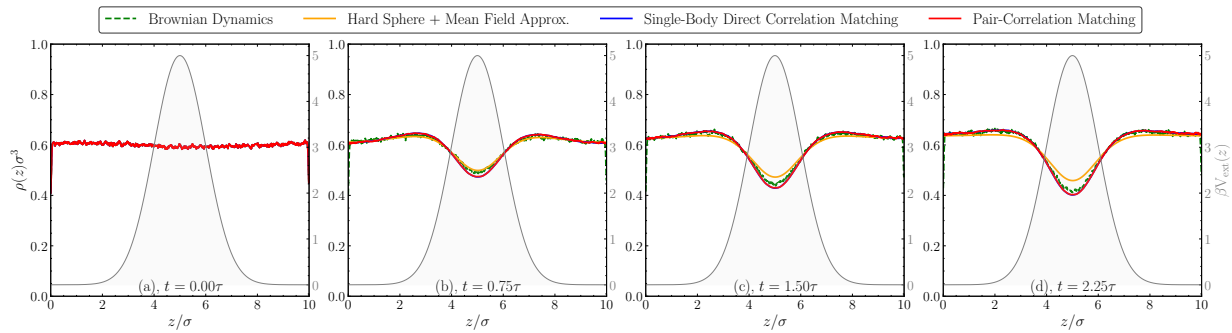


FIG. 2: Time evolution of the one-body density profile  $\rho(z, \tau)$  for a system of interacting 3D LJ particles with planar geometry subjected to a repulsive Gaussian potential  $V_{\text{ext}}(z)$  (grey curve, right axis). The plots compare two neural excess free-energy functionals and an analytical FMT functional, with a reference Brownian dynamics simulation. Initially ( $t = 0\tau$ ), the system is at equilibrium with a flat density profile. Upon application of the external potential, the density profile evolves non-trivially, exhibiting a depletion near the potential maximum and eventually approaching a new equilibrium. The neural DDFT approaches (red and blue) exhibit good agreement with Brownian dynamics throughout the temporal evolution, notably with the pair-correlation matching approach (red) not having seen any inhomogeneous densities during training.

$$\frac{\partial \rho(\mathbf{r}, t)}{\partial t} = - \left( V_{\text{ext}} + \frac{1}{\beta} \ln(\Lambda^3 \rho(\mathbf{r}, t)) + \frac{\delta \mathcal{F}_{\text{exc}}[\rho(\mathbf{r}, t)]}{\delta \rho(\mathbf{r}, t)} - \mu \right) \rho(\mathbf{r}, t). \quad (10)$$

Note that the steady-state solution of this PDE (considering the total  $\mathcal{F}[\rho]$ ),

$$\left\| \nabla \frac{\delta \mathcal{F}[\rho(\mathbf{r}, t)]}{\delta \rho(\mathbf{r}, t)} \right\| = 0 \iff \frac{\delta \mathcal{F}[\rho(\mathbf{r}, t)]}{\delta \rho(\mathbf{r}, t)} = \mu, \quad (11)$$

is equivalent to the equilibrium density provided by the Euler-Lagrange equation in cDFT and hence it can also be interpreted as a continuous-time PDE alternative to Picard iterations.

## V. IMPLEMENTATION

We now describe the numerical implementation of our neural DDFT approach in relation to a Brownian dynamics (BD) reference simulation, where BD is chosen rather than (ballistic) molecular dynamics to be consistent with the overdamped nature of DDFT.

### A. Brownian dynamics

We use LAMMPS [29] to simulate BD motion of Lennard-Jones (LJ) particles under repulsive external fields. The motion is specified by the following overdamped Langevin equation,

$$d\mathbf{r} = \gamma^{-1} \mathbf{F} dt + \sqrt{2k_B T \gamma^{-1}} d\mathbf{W}_t, \quad (12)$$

where  $\gamma$  is the mobility coefficient,  $\mathbf{F}$  is the force acting on the particle, and  $d\mathbf{W}_t$  is a Wiener process.

We run BD simulations inside a closed 3D cube box of edge length  $10\sigma$  with periodic boundary conditions on all axes. We randomly initialize 600 LJ particles (with a cut-off distance of  $4\epsilon$ ) inside the box.  $\epsilon$  and  $\sigma$  are the LJ coefficients of well-depth and particle diameter respectively. The temperature of the system is kept at a constant  $k_B T / \epsilon = 2$  and each timestep is  $10^{-3}\tau$  where  $\tau$  is the time scale  $\gamma\sigma^2/\epsilon$  and  $\gamma$  is the mobility coefficient.

We first run an energy minimization to adjust the random initial configuration to be in a local energy minimum with tolerance  $10^{-4}\epsilon$ , followed by 2000 equilibration steps which results in a uniform density distribution. We then apply an external potential (mixture of repulsive Gaussian and steep well) on this system, using a PyLAMMPS extension [30], and run 4000 collection steps ( $4\tau$ ) with the thermodynamic output variables averaged over 10 steps. The density is collected every 10 steps, averaged over a bin size of  $\sigma/100$  along the  $z$ -axis and across the  $xy$  plane, assuming planar geometry. We further average over 5000 BD runs to obtain smooth density profiles.

### B. Dynamical density functional theory

We numerically integrate the DDFT equation (Eq. (3)), with the neural excess free-energy functional from pair-correlation matching,

$$\frac{\partial \rho(\mathbf{r}, t)}{\partial t} = \Gamma \nabla \cdot \left[ \rho(\mathbf{r}, t) \nabla \cdot \left( \frac{\delta \mathcal{F}_{\theta, \text{exc}}[\rho]}{\delta \rho(\mathbf{r}, t)} + V_{\text{ext}}(\mathbf{r}, t) + \frac{1}{\beta} \ln(\Lambda^3 \rho(\mathbf{r}, t)) \right) \right], \quad (13)$$

to obtain time-dependent density profiles of 3D Lennard-Jones (LJ) systems with planar geometry under an external potential  $V_{\text{ext}}$  (Fig. 1).

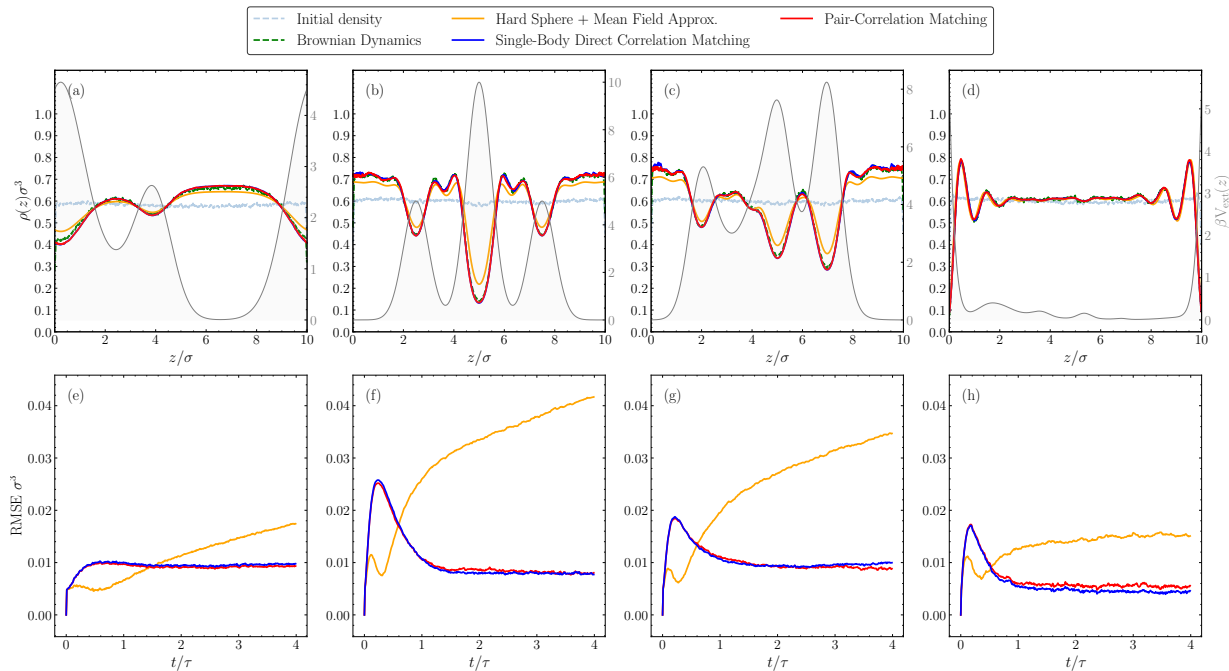


FIG. 3: The final equilibrium density profiles and their RMSE over time evolution under complex external potentials (see Appendix E for the movie version). (a)-(d) A comparison of the final 1D equilibrium density profiles for a three-dimensional LJ system with planar geometry under different external potentials constructed from sums of repulsive Gaussian and steep well potentials. (e)-(h) show the corresponding RMSE deviation from the Brownian dynamics results over time evolution. The densities obtained with the neural functionals are significantly more accurate than those with the analytical functional, notably with the pair-correlation matching approach (red) not having seen any inhomogeneous densities during training.

We define a 1D density grid of  $10\sigma$  length with a spacing of  $\sigma/100$  for the solver, with periodic boundaries. We initialize the density grid with the same uniform initial density as the reference BD simulation and apply the same external potential. We simulate the PDE with a time-step of  $10^{-4}\tau$  until  $t = 4\tau$ , where  $\tau = \sqrt{m\sigma^2/\epsilon}$  in reduced LJ units. The gradients are computed using finite-differences and time integrated using an Euler scheme, as implemented in the numerical Py-PDE Python package [31]. A pseudospectral solver can also be used for scenarios that require more numerical precision [32]. The mobility coefficient  $\Gamma$  is chosen to be the same as in BD. For computing  $\delta\mathcal{F}_{\theta,\text{exc}}[\rho(\mathbf{r}, t)]/\delta\rho(\mathbf{r}, t)$ , we use automatic differentiation over the excess neural free-energy functional.

## VI. EXPERIMENTS

We run two sets of “experiments” to evaluate the accuracy and efficiency of neural DDFT from pair-correlation matching with respect to BD, one on a closed system with planar geometry and conserved number of particles under various external potentials, and the other on an open system with a source and sink with varying number of particles, inspired by a gas adsorption process.

### A. Closed system

We use a 3D system of LJ particles with planar geometry, under external potentials that are mixtures of repulsive Gaussian and steep well potentials as in [10]. In addition to the neural functional from pair-correlation matching (denoted by  $\mathcal{F}_{\theta,\text{exc}}^{(2)}$ ), we also train a functional using single-body direct correlation matching (denoted by  $\mathcal{F}_{\theta,\text{exc}}^{(1)}$ ) (see Appendix A 1). Both functionals use the same convolutional neural network with periodic and dilated convolutions, each with a kernel size of 3, a dilation of 2, and 6 layers. The layer dimensions are set to  $N_{\text{channels}} = [16, 16, 32, 32, 64, 64]$ , with average pooling with kernel size 2 applied after each layer. The models are trained for 5000 epochs, each taking less than an hour on an RTX 4070 GPU for convergence.

For training  $\mathcal{F}_{\theta,\text{exc}}^{(2)}$ , we simulated 1000 *uniform* densities and measured their radial distribution functions with  $\sigma/100$  grid-size and chemical potentials in the range  $-4$  to  $0.5$ .  $\mathcal{F}_{\theta,\text{exc}}^{(1)}$  is trained on 800 non-uniform densities [10] with  $\sigma/100$  grid-size and chemical potentials in the range  $-4$  to  $0.5$ . The dataset of  $\mathcal{F}_{\theta,\text{exc}}^{(2)}$  is larger, since no validation set had to be excluded from the train set, since it is validated on samples from the non-uniform dataset. We also evaluate against an analytical functional  $\mathcal{F}_{\text{exc}}^{\text{MF}}$  which models the attractive contribution using mean-

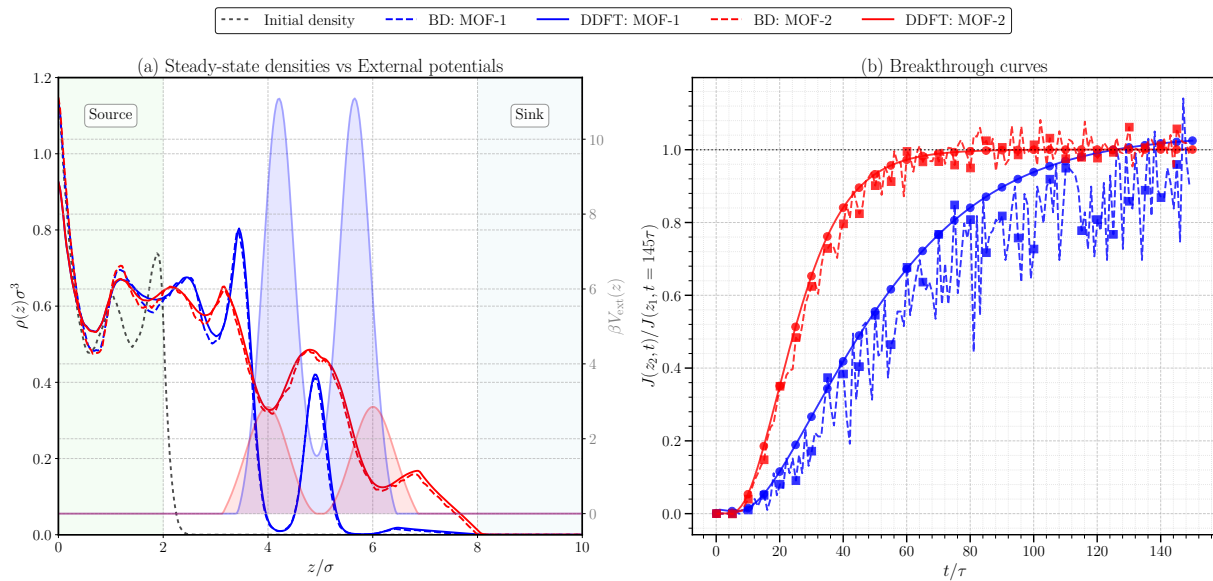


FIG. 4: Breakthrough simulations using neural DDFT and Brownian dynamics (see Appendix E for the movie version). (a) LJ particles from the source move towards the sink under two different MOF-like repulsive external potentials. The dynamics of the density evolution and the final evolved density (visualized) obtained from DDFT are in close agreement with BD. (b) Time evolution of the output to input flux ratio, showing the approach towards steady-state or breakthrough condition. The particles reach breakthrough earlier under the MOF-2 external potential. The curves obtained from DDFT are in close agreement with BD, while being smoother and taking only 2% of the compute time of BD.

field approximation and the hard-sphere contribution using White-Bear II version of FMT [33], as implemented in PyDFTlj [1].

Our experiments show that the neural free energy functionals  $\mathcal{F}_{\theta, \text{exc}}^{(1)}$  and  $\mathcal{F}_{\theta, \text{exc}}^{(2)}$  are both significantly better than the  $\mathcal{F}_{\text{exc}}^{\text{MF}}$  functional in accuracy across time, as shown in Fig. 2 & Fig. 3. The convergence of  $\mathcal{F}_{\theta, \text{exc}}^{(2)}$  is similar to  $\mathcal{F}_{\theta, \text{exc}}^{(1)}$ , except in Fig. 3(d) where the density near the wells is pushed above the maximum bulk value of  $0.67\sigma^{-3}$  seen during training of  $\mathcal{F}_{\theta, \text{exc}}^{(2)}$ . The errors for all the DDFT approaches for time intervals  $t < 1\tau$  are high which we attribute to overly fast dynamics arising from the adiabatic approximation [22]. More notably, the dynamical density profiles from DDFT are several orders of magnitude faster to compute with DDFT than with BD simulation: while running 5000 trials of BD takes about a day on a single-core CPU, the DDFT approach on the same computer takes less than 6 minutes (see Appendix D for runtime comparisons).

## B. Open system

To evaluate the pair-correlation matching functional  $\mathcal{F}_{\theta, \text{exc}}^{(2)}$  on an open system, we construct a system modeled after “breakthrough” experiments used in gas adsorption studies [34, 35]. In these studies, typically a column filled with adsorbent material (e.g. nanoporous metal-organic framework (MOF) is exposed to a gas stream (e.g.  $\text{CO}_2$ ),

where the breakthrough of the gas is detected at the outlet to estimate the adsorption capacity and kinetics of the material. We adopt such a setup by extending the closed Lennard-Jones system from the previous experiment with two particle baths, one at a high  $\mu = 0.5$  in  $z \in [0, 2]\sigma$  to simulate an LJ particle source and the other at extremely low  $\mu = -100$  in  $z \in [8, 10]\sigma$  to simulate an LJ particle sink. The difference in  $\mu$  causes particles to flow from the source to the sink through the region  $z \in [2, 8]\sigma$ , in which we apply, in addition, a planar potential to mimic two MOF planes from the IRMOF series [36] (see Appendix C). In the reference BD simulation, we extend the closed system to an open system by attaching two Grand-Canonical Monte-Carlo (GCMC) reservoirs as source and sink. The source reservoir is from  $z = [0, 2]\sigma$  with  $\mu = 0.5$  and the sink is from  $z = [8, 10]\sigma$  with  $\mu = -100$ . 10 trials of GCMC insertion/deletion steps, with no translation/rotation, are attempted in LAMMPS (hybrid) between every BD update. Before starting the breakthrough simulation, we first randomly initialize LJ particles in the source region and confine them using a potential barrier and equilibrate the system for 20000 steps (each timestep is  $10^{-3}\tau$ ). Then the barrier is removed and the MOF-like potential is applied on the system and 100000 collection steps are performed as the particles flow towards the sink. The planar density is sampled every 100 steps, over a bin size of  $\sigma/32$  and is averaged over 500 BD runs.

We simulate this same system using our open DDFT equation (Eq. (8)) for a duration of  $150\tau$ , with a timestep of  $10^{-3}\tau$  and grid spacing of  $\sigma/32$ . To obtain break-

through curves we compute the time-dependence of the ratio  $J(z_2, t)/J(z_1, T)$  of the particle fluxes  $J(z_2, t)$  close to the output at  $z_2 = 7.5\sigma$  and  $J(z_1, T)$  close to the input at  $z_1 = 2.5\sigma$  at late time  $T = 145\tau$  where steady-state is (almost) reached. The particle flux from DDFT is computed as  $J(z, t) = -\Gamma\rho(z, t)\nabla(\delta\mathcal{F}[\rho(z)]/\delta\rho(z))$ , where  $\mathcal{F}_{\theta, \text{exc}}^{(2)}$  is used for the excess component. We also apply a Savitsky-Golay filter [37] over the spatial gradient in the flux computation to smooth out any noise arising from numerical errors. The BD flux is computed as the net number of particles crossing the planes at  $z_1$  and  $z_2$  per unit time per unit area, averaged over 500 BD runs.

As observed from the breakthrough curves in Fig. 4, the dynamics of both the BD and DDFT simulations agree closely and reach breakthrough at similar times. The potential from MOF-2 (red), which corresponds to a MOF with larger pore size, presents a lower particle barrier giving rise to a faster evolution to the steady state, which is captured by both simulations. But the DDFT simulation is much more efficient, taking only 2% of the compute time of the BD simulation (see Appendix D for runtime comparisons). Note that since the GCMC moves are run in between each BD update while the open DDFT equation updates are simultaneous, we do not expect exact dynamical agreement though this can be alleviated to some extent with the choice of  $\Gamma'$  in the growth term.

## VII. CONCLUSION

To summarize, we have presented results that the neural excess free-energy functional trained via pair-correlation matching can be directly applied to DDFT without retraining, with high accuracy relative to an analytical free-energy approximation and with high efficiency relative to BD simulations. We show this for both conserved dynamics, as well as for non-conserved dynamics via a novel gradient flow based extension which we evaluate on a system inspired by breakthrough adsorption simulations. Future work could focus on the extension of this method to systems with full 3D geometry and anisotropic particles, and extending it to incorporate superadiabatic forces [38], towards practical applications in modeling many-body non-equilibrium systems.

## ACKNOWLEDGEMENTS

We would like to thank David Dubbeldam and Christian Koke for useful discussions.

## DATA AVAILABILITY

Code and data to reproduce all results will be made available upon publication.

## Appendix A: Classical Density Functional Theory

Classical density functional theory (cDFT) [3] proves the existence of a grand potential functional  $\Omega[\rho]$  of a one-body density profile  $\rho(\mathbf{r})$ , with the condition that the equilibrium density profile  $\rho_{\text{eq}}(\mathbf{r})$  minimizes  $\Omega[\rho]$  and is equal to the equilibrium grand potential  $\Omega_0$ . From  $\Omega_0$ , all the thermodynamic properties of the system of interest can be subsequently derived.

$$\left. \frac{\partial\Omega(\mu, [\rho], T)}{\partial\rho(\mathbf{r})} \right|_{\rho=\rho_{\text{eq}}} = 0, \quad \Omega([\rho_{\text{eq}}]) = \Omega_0. \quad (\text{A1})$$

The grand potential functional  $\Omega[\rho]$  can be written as,

$$\Omega(\mu, [\rho], T) = \mathcal{F}([\rho], T) - \int d^3r \rho(\mathbf{r})(\mu - V_{\text{ext}}(\mathbf{r})), \quad (\text{A2})$$

where  $\mu$  is the chemical potential,  $T$  is the temperature, and  $\mathcal{F}[\rho]$  is the intrinsic Helmholtz free-energy functional which can be split into three parts,

$$\mathcal{F}([\rho], T) = \mathcal{F}_{\text{id}}([\rho], T) + \mathcal{F}_{\text{ext}}([\rho], T) + \mathcal{F}_{\text{exc}}([\rho], T), \quad (\text{A3})$$

where  $\mathcal{F}_{\text{id}}([\rho], T) = \frac{1}{\beta} \int d^3\mathbf{r} \rho(\mathbf{r})(\ln(\Lambda^3 \rho(\mathbf{r})) - 1)$ ,  $\beta = (1/k_B T)$  and  $\Lambda$  is the thermal wavelength, and  $\mathcal{F}_{\text{ext}}([\rho]) = \int d^3\mathbf{r} \rho(\mathbf{r}) V_{\text{ext}}(\mathbf{r})$ .

The challenge is to approximate  $\mathcal{F}_{\text{exc}}[\rho]$  which represents the inter-particle interactions as a functional of the non-local density. Once such an  $\mathcal{F}[\rho]$  is (approximately) obtained, the equilibrium density  $\rho_{\text{eq}}(\rho)$  from Eq. A1 can be formulated as the following Euler-Lagrange equation,

$$\rho_{\text{eq}}(\mathbf{r}) = \frac{1}{\Lambda^3} \exp \left( \beta\mu - \beta \left. \frac{\delta\mathcal{F}_{\text{exc}}[\rho]}{\delta\rho(\mathbf{r})} \right|_{\rho=\rho_{\text{eq}}} - \beta V_{\text{ext}}(\mathbf{r}) \right). \quad (\text{A4})$$

This self-consistency relation can be solved by means of a recursive Picard iteration scheme to compute the equilibrium density starting from any arbitrary initial density. It is also worth noting that cDFT can be interpreted as a grand-canonical framework in which the system is in thermal and diffusive equilibrium with a particle bath at chemical potential  $\mu$  and temperature  $T$ .

### 1. Single-Body Direct Correlation Matching

In addition to pair-correlation matching [10], we can also train a neural free-energy functional ( $\mathcal{F}_{\theta, \text{exc}}^{(1)}$ ) using single-body direct correlation matching. This is done by minimizing the error between the target  $\delta\mathcal{F}_{\text{exc}}/\delta\rho(z_i)$  and the estimate  $(1/\Delta z)\partial\mathcal{F}_{\theta, \text{exc}}^{(1)}/\partial\rho_i$ . This functional derivative of the excess free-energy is the one-body direct correlation function, and computing the target samples requires simulating inhomogeneous equilibrium densities under a range of external potentials.

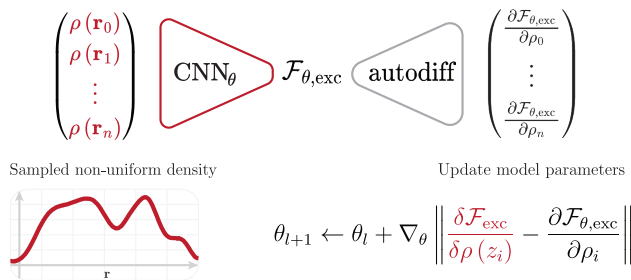


FIG. 5: An overview of single-body direct correlation matching.

## Appendix B: Dynamical Density Functional Theory

We provide here a phenomenological derivation for classical dynamical density functional theory (DDFT) starting from cDFT, originally presented by Evans [3]. DDFT can also alternatively be derived from Langevin equations [11], Smoluchowski equations [12], as well as from a projection operator formalism [39]. Consider the continuity equation for conserved  $\rho$ ,

$$\frac{\partial \rho(\mathbf{r}, t)}{\partial t} + \nabla \cdot \mathbf{J}(\mathbf{r}, t) = 0. \quad (\text{B1})$$

Considering the flux  $\mathbf{J}(\mathbf{r}, t) = \rho(\mathbf{r}, t)\mathbf{v}(\mathbf{r}, t)$ ,

$$\frac{\partial \rho(\mathbf{r}, t)}{\partial t} + \nabla \cdot (\rho(\mathbf{r}, t)\mathbf{v}(\mathbf{r}, t)) = 0, \quad (\text{B2})$$

where the average velocity  $\mathbf{v}(\mathbf{r}, t) = -\Gamma \nabla \mu(\mathbf{r}, t)$  with the mobility coefficient  $\Gamma$ . Expanding this we get,

$$\frac{\partial \rho(\mathbf{r}, t)}{\partial t} - \Gamma \nabla \cdot (\rho(\mathbf{r}, t) \nabla \mu(\mathbf{r}, t)) = 0. \quad (\text{B3})$$

From cDFT, we know at equilibrium  $\mu = \delta \mathcal{F}[\rho(\mathbf{r})] / \delta \rho(\mathbf{r})$ . This equilibrium density functional can also be applied to DDFT close to equilibrium. This leads to,

$$\frac{\partial \rho(\mathbf{r}, t)}{\partial t} = \Gamma \nabla \cdot \left[ \rho(\mathbf{r}, t) \nabla \left( \frac{\delta \mathcal{F}[\rho(\mathbf{r}, t)]}{\delta \rho(\mathbf{r}, t)} \right) \right]. \quad (\text{B4})$$

Re-arranging the terms and expanding the free-energy functional we get,

$$\frac{\partial \rho(\mathbf{r}, t)}{\partial t} = \Gamma \nabla \cdot \left[ \rho(\mathbf{r}, t) \nabla \left( \frac{\delta \mathcal{F}_{\text{exc}}[\rho]}{\delta \rho(\mathbf{r}, t)} + V_{\text{ext}}(\mathbf{r}, t) + \frac{1}{\beta} \ln(\Lambda^3 \rho(\mathbf{r}, t)) \right) \right]. \quad (\text{B5})$$

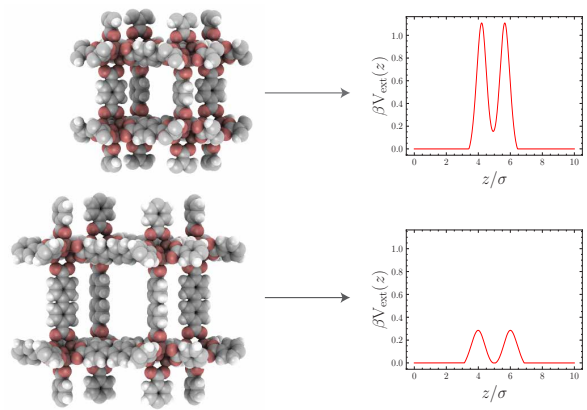


FIG. 6: IRMOF-1 (top) and IRMOF-10 (bottom) and their corresponding effective 1D potentials computed along the pore axes.

## Appendix C: MOF-like planar potentials

Here we describe our procedure for obtaining the 1D external potentials from metal-organic frameworks (MOF) for the breakthrough simulation experiment in the main paper.

We use the IRMOF-1 and IRMOF-10 structures from the IRMOF series of crystal structures [36], which have the same topology but differing pore sizes. To convert their 3D structures into effective 1D external potentials suitable for DDFT, we employed a simulation-based force sampling approach using LAMMPS [29]. Starting from CIF files of the MOFs, we generated compatible data files for LAMMPS with appropriate force field assignments and topology using lammps-interface [40]. The pore axis of each MOF was aligned along the  $z$ -direction, and a single LJ-type guest particle was introduced and displaced incrementally along its pore axis and the total force acting on it was recorded at each step. This produced a raw force profile as a function of  $z$ -position which was then converted to reduced LJ units and numerically integrated (in reverse) to generate a dimensionless potential profile. The resulting potentials were clipped and centered to remove artifacts at the boundaries and padded with zeros to enforce a flat, finite domain. The final 1D potentials, expressed as functions interpolated over a grid, serve as external fields  $V_{\text{ext}}$  that approximate the confinement environment of the original MOF pores.

## Appendix D: Runtime comparisons

The below table is a comparison of *approximate* runtimes between BD simulation and our DDFT implementation for open and closed systems across two different grid sizes. While each DDFT simulation directly produces smooth density profiles, each BD simulation needs to be ensemble averaged (over 5000 and 500 runs for

closed and open resp.), to obtain comparable density profiles. Both simulations were run on a single-core of Intel(R) Xeon(R) W-2123 CPU @ 3.60GHz or comparable CPU. Note that DDFT uses  $\Delta t = 10^{-3}\tau$  for grid spacing  $\sigma/32$  and  $\Delta t = 10^{-4}\tau$  for grid spacing  $\sigma/100$ , while BD uses  $\Delta t = 10^{-3}\tau$  for both.

System	Grid	BD	DDFT
Closed (Eq. (M1), until $t = 4\tau$ )	$\sigma/32$	34 hours	25 secs.
	$\sigma/100$	34 hours	5 mins.
Open (Eq. (M2), until $t = 150\tau$ )	$\sigma/32$	48 hours	40 mins.
	$\sigma/100$	48 hours	8 hours

## Appendix E: Supplemental Movies

We also attach two movie files as supplemental material (also available on the project webpage [41]).

*dynamical-density-profiles.mp4*: Dynamical version of Fig. (3) showing the density profiles in the main paper.

*breakthrough-simulation.mp4*: Dynamical version of Fig. (4) showing the breakthrough curves in the main paper.

- 
- [1] E. d. A. Soares, A. G. Barreto, and F. W. Tavares, Classical density functional theory reveals structural information of H<sub>2</sub> and CH<sub>4</sub> fluids adsorbed in MOF-5, *Fluid Phase Equilibria*, 113887 (2023).
- [2] Q. Wei, T. Becherer, S. Angioletti-Uberti, J. Dzubiella, C. Wischke, A. T. Neffe, A. Lendlein, M. Ballauff, and R. Haag, Protein interactions with polymer coatings and biomaterials, *Angewandte Chemie International Edition* **53**, 8004 (2014).
- [3] R. Evans, The nature of the liquid-vapour interface and other topics in the statistical mechanics of non-uniform, classical fluids, *Advances in physics* **28**, 143 (1979).
- [4] J.-P. Hansen and I. R. McDonald, *Theory of simple liquids: with applications to soft matter* (Academic press, 2013).
- [5] Y. Rosenfeld, Free-energy model for the inhomogeneous hard-sphere fluid mixture and density-functional theory of freezing, *Physical review letters* **63**, 980 (1989).
- [6] S. C. Lin and M. Oettel, A classical density functional from machine learning and a convolutional neural network, *SciPost Physics* **6**, 1 (2019), arXiv:1811.05728.
- [7] P. Cats, S. Kuipers, S. de Wind, R. van Damme, G. M. Coli, M. Dijkstra, and R. van Roij, Machine-learning free-energy functionals using density profiles from simulations, *APL Materials* **9**, 031109 (2021).
- [8] F. Sammüller, S. Hermann, D. de las Heras, and M. Schmidt, Neural functional theory for inhomogeneous fluids: Fundamentals and applications, *Proceedings of the National Academy of Sciences* **120**, e2312484120 (2023).
- [9] A. Simon, J. Weimar, G. Martius, and M. Oettel, Machine Learning of a Density Functional for Anisotropic Patchy Particles, *Journal of Chemical Theory and Computation* **20**, 1062 (2024).
- [10] J. Dijkman, M. Dijkstra, R. van Roij, M. Welling, J.-W. van de Meent, and B. Ensing, Learning neural free-energy functionals with pair-correlation matching, *Phys. Rev. Lett.* **134**, 056103 (2025).
- [11] U. M. B. Marconi and P. Tarazona, Dynamic density functional theory of fluids, *The Journal of Chemical Physics* **110**, 8032 (1999).
- [12] A. J. Archer and R. Evans, Dynamical density functional theory and its application to spinodal decomposition, *The Journal of chemical physics* **121**, 4246 (2004).
- [13] M. te Vrugt, H. Löwen, and R. Wittkowski, Classical dynamical density functional theory: from fundamentals to applications, *Advances in Physics* **69**, 121 (2020).
- [14] A. Diaw and M. Murillo, A dynamic density functional theory approach to diffusion in white dwarfs and neutron star envelopes, *The Astrophysical Journal* **829**, 16 (2016).
- [15] A. M. Menzel, A. Saha, C. Hoell, and H. Löwen, Dynamical density functional theory for microswimmers, *The Journal of chemical physics* **144**, 10.1063/1.4939630 (2016).
- [16] M. Te Vrugt and R. Wittkowski, Perspective: New directions in dynamical density functional theory, *Journal of Physics: Condensed Matter* **35**, 041501 (2022).
- [17] L. Ambrosio, N. Gigli, and G. Savaré, *Gradient flows: in metric spaces and in the space of probability measures* (Springer Science & Business Media, 2008).
- [18] K. Neklyudov, J. Nys, L. Thiede, J. Carrasquilla, Q. Liu, M. Welling, and A. Makhzani, Wasserstein quantum monte carlo: a novel approach for solving the quantum many-body schrödinger equation, *Advances in Neural Information Processing Systems* **36**, 10.48550/arXiv.2307.07050 (2024).
- [19] M. Raissi, P. Perdikaris, and G. Karniadakis, Physics-informed neural networks: A deep learning framework for solving forward and inverse problems involving nonlinear partial differential equations, *Journal of Computational Physics* **378**, 686 (2019).
- [20] M. Schmidt and J. M. Brader, Power functional theory for brownian dynamics, *The Journal of Chemical Physics* **138**, 214101 (2013).
- [21] M. Schmidt, Power functional theory for many-body dynamics, *Rev. Mod. Phys.* **94**, 015007 (2022).
- [22] S. M. Tschoop and J. M. Brader, First-principles superadiabatic theory for the dynamics of inhomogeneous fluids, *The Journal of Chemical Physics* **157**, 234108 (2022).
- [23] G. S. Heffelfinger and F. v. Swoll, Diffusion in lennard-jones fluids using dual control volume grand canonical molecular dynamics simulation (dcv-gcmd), *The Journal of chemical physics* **100**, 7548 (1994).
- [24] A. Ozcan, C. Perego, M. Salvalaglio, M. Parrinello, and O. Yazaydin, Concentration gradient driven molecular dynamics: a new method for simulations of membrane permeation and separation, *Chem. Sci.* **8**, 3858 (2017).

- [25] U. Thiele, I. Vancea, A. J. Archer, M. J. Robbins, L. Fratista, A. Stannard, E. Pauliac-Vaujour, C. P. Martin, M. O. Blunt, and P. J. Moriarty, Modelling approaches to the dewetting of evaporating thin films of nanoparticle suspensions, *Journal of Physics: Condensed Matter* **21**, 264016 (2009).
- [26] J.-D. Benamou and Y. Brenier, A computational fluid mechanics solution to the monge-kantorovich mass transfer problem, *Numerische Mathematik* **84**, 375 (2000).
- [27] R. Jordan, D. Kinderlehrer, and F. Otto, The variational formulation of the fokker-planck equation, *SIAM journal on mathematical analysis* **29**, 1 (1998).
- [28] L. Chizat, G. Peyré, B. Schmitzer, and F.-X. Vialard, An interpolating distance between optimal transport and fisher-rao metrics, *Foundations of Computational Mathematics* **18**, 1 (2018).
- [29] A. P. Thompson, H. M. Aktulga, R. Berger, D. S. Bolinteanu, W. M. Brown, P. S. Crozier, P. J. in 't Veld, A. Kohlmeyer, S. G. Moore, T. D. Nguyen, R. Shan, M. J. Stevens, J. Tranchida, C. Trott, and S. J. Plimpton, LAMMPS - a flexible simulation tool for particle-based materials modeling at the atomic, meso, and continuum scales, *Comp. Phys. Comm.* **271**, 108171 (2022).
- [30] K. Fazel, N. Karimitari, T. Shah, C. Sutton, and R. Sundararaman, Improving the reliability of machine learned potentials for modeling inhomogeneous liquids, *Journal of Computational Chemistry* **45**, 1821 (2024).
- [31] D. Zwicker, py-pde: A python package for solving partial differential equations, *Journal of Open Source Software* **5**, 2158 (2020).
- [32] A. Nold, B. D. Goddard, P. Yatsyshin, N. Savva, and S. Kalliadasis, Pseudospectral methods for density functional theory in bounded and unbounded domains, *Journal of Computational Physics* **334**, 639 (2017).
- [33] H. Hansen-Goos and R. Roth, Density functional theory for hard-sphere mixtures: the white bear version mark ii, *Journal of Physics: Condensed Matter* **18**, 8413 (2006).
- [34] D. Britt, H. Furukawa, B. Wang, T. G. Glover, and O. M. Yaghi, Highly efficient separation of carbon dioxide by a metal-organic framework replete with open metal sites, *Proceedings of the National Academy of Sciences* **106**, 20637 (2009).
- [35] S. Sharma, S. R. G. Balestra, R. Baur, U. Agarwal, E. Zuidema, M. S. Rigutto, S. Calero, T. J. H. Vlugt, and D. D. and, Ruptura: simulation code for breakthrough, ideal adsorption solution theory computations, and fitting of isotherm models, *Molecular Simulation* **49**, 893 (2023).
- [36] M. Eddaoudi, J. Kim, N. Rosi, D. Vodak, J. Wachter, M. O'Keeffe, and O. M. Yaghi, Systematic design of pore size and functionality in isoreticular mofs and their application in methane storage, *Science* **295**, 469 (2002).
- [37] A. Savitzky and M. J. E. Golay, Smoothing and differentiation of data by simplified least squares procedures., *Analytical Chemistry* **36**, 1627 (1964).
- [38] D. de las Heras, T. Zimmermann, F. Sammler, S. Hermann, and M. Schmidt, Perspective: How to overcome dynamical density functional theory, *Journal of Physics: Condensed Matter* **35**, 271501 (2023).
- [39] A. Yoshimori, Microscopic derivation of time-dependent density functional methods, *Physical Review E—Statistical, Nonlinear, and Soft Matter Physics* **71**, 031203 (2005).
- [40] P. G. Boyd, S. M. Moosavi, M. Witman, and B. Smit, Force-field prediction of materials properties in metal-organic frameworks, *The Journal of Physical Chemistry Letters* **8**, 357 (2017), pMID: 28008758.
- [41] Project webpage at <http://karnikram.info/neural-ddft-pcm>.